A Computational Study of Lower Urinary Tract Nerve Recruitment with Epidural Stimulation of the Lumbosacral Spinal Cord

Maria K. Jantz, Lucy Liang, Arianna Damiani, Lee E. Fisher, Taylor Newton, Esra Neufeld, T. Kevin Hitchens, Elvira Pirondini, Marco Capogrosso, Robert A. Gaunt

Abstract— **Bladder dysfunction is a major health risk for people with spinal cord injury. Recently, we have demonstrated that epidural sacral spinal cord stimulation (SCS) can be used to activate lower urinary tract nerves and provide both major components of bladder control: voiding and continence. To effectively control these functions, it is necessary to selectively recruit the afferents of the pudendal nerve that evoke these distinct bladder reflexes. Translation of this innovation to clinical practice requires an understanding of optimal electrode placements and stimulation parameters to guide surgical practice and therapy design. Computational modeling is an important tool to address many of these experimentally intractable stimulation optimization questions. Here, we built a realistic MRI-based finite element computational model of the feline sacral spinal cord which included realistic axon trajectories in the dorsal and ventral roots. We coupled the model with biophysical simulations of membrane dynamics of afferent and efferent axons that project to the lower urinary tract through the pelvic and pudendal nerves. We simulated the electromagnetic fields arising from stimulation through SCS electrodes and calculated the expected recruitment of pelvic and pudendal fibers. We found that SCS can selectively recruit pudendal afferents, in agreement with our experimental data in cats. Our results suggest that SCS is a promising technology to improve bladder function after spinal cord injury, and computational modeling unlocks the potential for highly optimized, selective stimulation.**

Clinical Relevance— **This model provides a method to non-invasively establish electrode placement and stimulation parameters for improving bladder function with epidural spinal cord stimulation.**

I. INTRODUCTION

Lower urinary tract dysfunction is one of the most significant yet most overlooked consequences of spinal cord injury. However, existing interventions to address this dysfunction are insufficient and only manage symptoms. Recently, we demonstrated in an animal model that epidural spinal cord stimulation (SCS) activates the nerves of the lower urinary tract [1] and evokes bladder reflexes that control both continence and voiding. In order to translate this technology to humans, it is critical to establish SCS locations and stimulation parameters to best target the bladder. Determining effective stimulation parameters clinically requires extensive testing with no guarantee of success because the pathways by which SCS produces bladder functions are not fully understood. Further, if the electrode is placed improperly, it may be impossible to evoke the desired bladder functions.

The primary nerves involved in lower urinary tract control are the pelvic and the pudendal nerves. The efferents of the pelvic nerve innervate the smooth muscle of the bladder and evoke contractions, while the afferents of the pelvic nerve signal bladder volume [2]. The efferents of the pudendal nerve evoke external urethral sphincter contractions, while the afferents signal sensory information from the urethra and genitalia [2]. Critically, activation of pudendal afferents with high-frequency (33 Hz) electrical stimulation can evoke voiding reflexes, while low-frequency (3 Hz) stimulation can evoke continence reflexes [3], [4]. Unfortunately, it is difficult to surgically access the pudendal nerve in humans [5], and it is therefore desirable to use SCS, which is a relatively low-invasive and established neuromodulation technology, to selectively activate the pudendal afferents. However, SCS can recruit afferents in many dorsal roots or in the dorsal columns [6] and it is therefore unknown whether it could lead to the selective activation of the pudendal afferents that is required for an effective therapy.

To address this question and facilitate parameter optimization, we generated a realistic computational model of the sacral spinal cord to explore neural activation of pudendal and pelvic afferents with SCS. Using data from ultra-high-resolution MRI and diffusion tensor imaging, we generated an anatomically realistic computational model of the cat sacral spinal cord and populated the computational model with hundreds of unique axon trajectories. We compared results of SCS at two electrode sites previously tested in cat experiments with simulated SCS at these sites in the computational model. We demonstrate here that we can use a computational model to find the expected activation of the pudendal afferents in agreement with experimental data, offering a path to optimize SCS electrode locations and stimulation parameters that will drive bladder function.

II. METHODS

We generated a simplified anatomical model of the cat sacral spinal cord based on MRI data and used Sim4Life 6.2 with NEURON to simulate an electromagnetic field in the tissue volume as well as the resulting activation of neural elements.

A. Model Overview

We obtained postmortem tissue and imaged a cat sacral spinal cord, spanning the L6 and L7 vertebra. The tissue was soaked in 0.2% Gadavist (gadolinium contrast agent) to reduce imaging time. It was then placed in Fomblin and the sample was imaged using a Bruker 11.7 Tesla/89 mm vertical-bore microimaging system. A 3D T$_2$-weighted anatomical scan was acquired at 50 µm isotropic resolution, which provided good contrast between tissues and facilitated rapid semiautomatic segmentation of gray matter, white matter, epidural fat, and CSF. In addition, a 3D high-resolution diffusion tensor imaging dataset was acquired (200 µm isotropic, 61 directions, multi-shell b=1000/3000) and tractography was employed to distinguish roots and rootlets of each spinal level.

From the MR images, we manually segmented 11 slices which spanned the caudal/rostral extent of the sample, smoothed the outlines of the segmented data in Adobe Illustrator 2020 and generated simplified volumes in Solidworks 2020 (Figure 1a). Surrounding the epidural fat layer, we generated a cylindrical volume designated as a bone layer, and a larger cylindrical volume modeled as saline. We generated an unstructured finite element mesh based on these volumes, using a maximum edge length of 0.2 mm in the gray matter, 0.5 mm in the white matter, 1 mm in the CSF and epidural fat, 2 mm in the bone, and 5 mm in the saline volume.

To model the electrode, we created a 0.291 mm x 1.0 mm x 0.05 mm volume with a silicone paddle backing and placed it above the CSF. We tested the electrode at two different locations on the spinal cord to match experimental data. The rostral electrode was positioned under the L6 vertebra and the caudal electrode under L7 vertebra (Figure 1a).

Using tractography, we produced 200 neural trajectories at each root level. To functionalize the model, we first assigned each neural trajectory to a specific nerve (pelvic, pudendal, sciatic, or other) according to literature values of these nerve distributions at each spinal level [7]–[10]. Next, we assigned a fiber diameter to each of these neurons by drawing randomly from probability distributions that were based on literature axon diameter distributions for each nerve [10], [11] (Figure 1b,c). Efferent and afferent neurons were assigned to the ventral and dorsal roots respectively.

B. Simulation

To prepare the model for simulation of the electromagnetic field produced by stimulation, we set electrical properties for each tissue layer. Uniform conductivity values for each tissue layer were set to 0.23 S/m in the gray matter, 1.7 S/m in the CSF, 0.04 S/m in the epidural fat, 0.02 S/m in the bone, and 2 S/m in the saline [6]. In the white matter, we set anisotropic conductivity to 0.083 S/m in the transverse directions and 0.6 S/m in the longitudinal direction [6]. On the outer surface of the saline, we set a Dirichlet boundary condition. We generated a simulation of the electromagnetic field produced by a biphasic stimulation pulse on this electrode at 1 mA with a pulse width of 0.2 ms in each phase.

Using the stimulated electric potential values, we determined the recruitment of each neuron in the model. Because these potential values are linearly scalable, we were also able to determine the amplitude at which each nerve was recruited. Neuron models were generated using the integrated
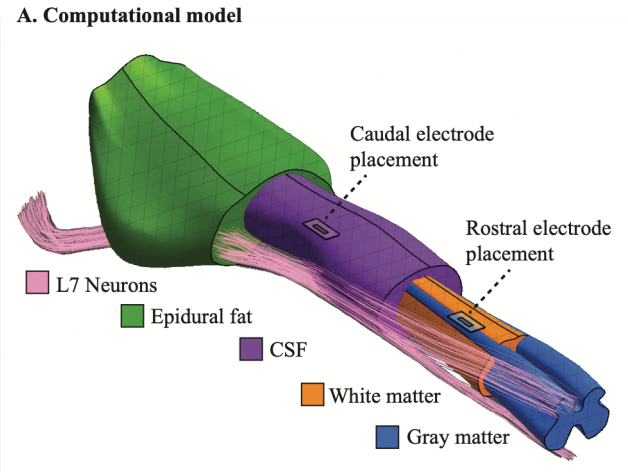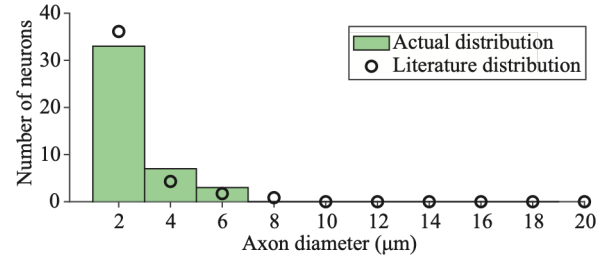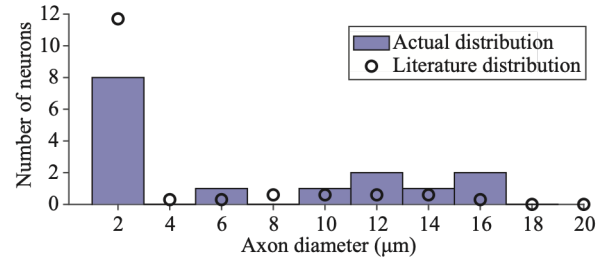

Figure 1. A. The simplified three-dimensional computational model, showing the gray matter, white matter, CSF, and epidural fat that were generated based on MRI data. Neuron traces generated based on DTI data are shown for the L7 roots on the right side of the cord only for clarity. Simulations were generated with electrodes at the shown rostral and caudal electrode placements, which are inside the epidural fat layer. B. Neuron diameter distribution generated for the pelvic nerve for a single run of the simulation based on the literature values shown. C. Neuron size distribution generated for the pudendal nerve for a single run of the simulation based on the literature values shown.

NEURON package in Sim4Life. Neurons larger than 4 µm in diameter were modeled based on the McIntyre-Richardson-Grill models of sensory and motor neurons [12]. Neurons between 2 µm and 4 µm in diameter were modeled as an adapted version of this model for small diameter myelinated axons [12], [13]. Neurons smaller than 2 µm were modeled as the peripheral axonal portion of unmyelinated neurons based on the Sundt model [14].

Experimental data used for validation of model results had been previously collected in 6 cats. In these experiments, we stimulated using a 24-channel SCS array (Micro-Leads, Inc.) and recorded action potentials from nerve cuffs (Micro-Leads, Inc.) on the pelvic, pudendal, and sciatic nerves [1]. In the

A. Simulated Rostral Recruitment

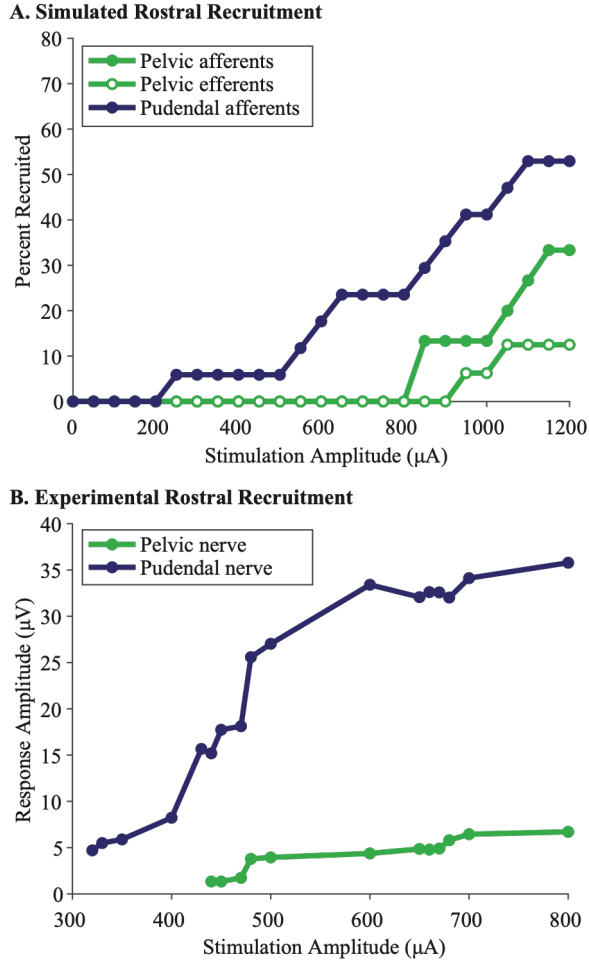**B. Experimental Rostral Recruitment**

Figure 2. Representative examples of pelvic and pudendal nerve recruitment at the rostral electrode placement. A. Pudendal afferents selectively recruited in our computational model. B. Pudendal nerve selectively recruited using SCS in a cat.

experimental work, electrode placements included a location in line with the L6 vertebra and a location in line with the L7 vertebra. Using anatomical landmarks in the MR images, the simulation electrode placements were matched to these two electrode placements in the experimental work.

III. RESULTS

We simulated recruitment curves for the pelvic and pudendal afferents, as well as the pelvic efferents, as these neural elements are the most critical in determining bladder reflex outcomes [15]. We then compared these results with our experimental data in cats.

A. Selective pudendal afferent recruitment

In our model, it was possible to recruit both the pelvic and pudendal afferent fibers with SCS at amplitudes similar to those shown experimentally. Most importantly, we could achieve selective pudendal afferent recruitment in both the computational model and in experiments. Figure 2a shows an example recruitment curve generated at the rostral placement in the computational model. Figure 2b shows an example recruitment curve generated at that same electrode placement selective for the pudendal nerve generated by SCS in a cat [1].
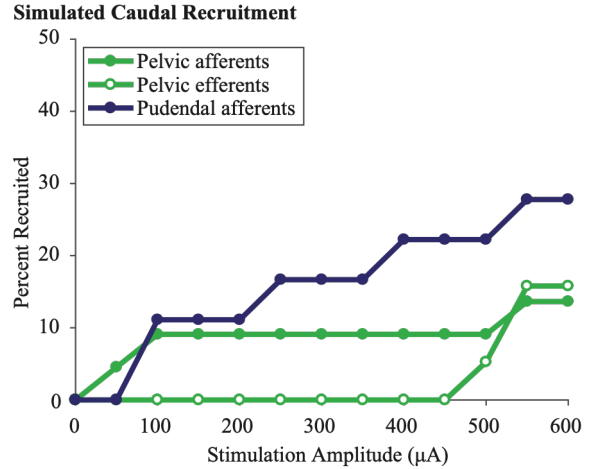
Simulated Caudal Recruitment

Figure 3. Representative example of pelvic and pudendal recruitment with simulated SCS at the caudal electrode placement. Pelvic afferents were selectively recruited in this example.

At the rostral location, the pelvic afferents were typically recruited at a higher amplitude than the pudendal afferents. Further, at this electrode placement it was typical to recruit afferent activity at much lower thresholds than efferent activity (Figure 2a), which is a question we were not able to address experimentally.

B. Selectivity at a caudal electrode site

At more caudal locations, including over the cauda equina, the increased volume of highly-conductive CSF and decreased volume of the spinal cord altered recruitment patterns. At this location, afferent recruitment thresholds were lower than at the rostral location. In Figure 3, a representative example demonstrates a typical recruitment profile at the caudal placement. In this example, the pelvic afferents were recruited selectively at 50 µA, and pudendal afferents were recruited at 100 µA. Simulations at the caudal location typically produced pelvic and pudendal afferent recruitment within 100 µA of each other.

C. Dynamic range between afferents and efferents

In order to maximize the relevant afferent recruitment, it is useful to know the full range of amplitudes at which we can stimulate with SCS before recruiting efferent activity. At both locations, efferent axons were recruited at a higher amplitude than the afferents. In 7 simulations at the rostral and the caudal placements, we determined the threshold for afferents and efferents and found that afferents were always recruited at lower stimulus amplitudes (Figure 4).

IV. DISCUSSION

In this study, we developed an anatomically accurate finite element model of the lumbosacral spinal cord of the cat to study recruitment of lower urinary tract afferent and efferent fibers. Pudendal afferent recruitment is necessary to produce bladder reflexes, and we demonstrate here that we can simulate recruitment of these fibers with SCS, in agreement with experimental evidence.

Pelvic afferents are often recruited in combination with pudendal afferents. Pelvic afferent activation in conjunction
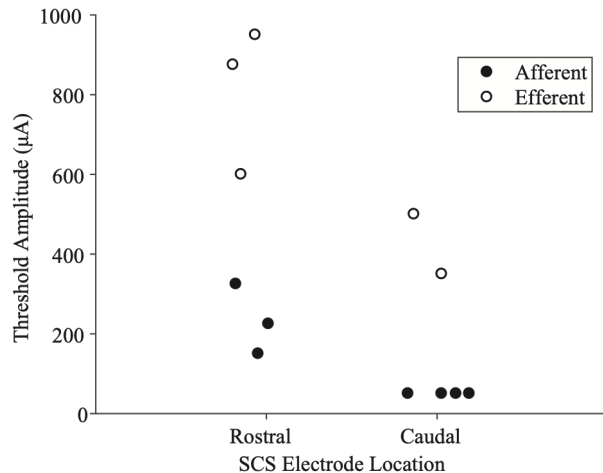
Figure 4. Threshold recruitment amplitudes in the computational model for afferents and efferents at the rostral and caudal electrode placements. In two simulations, pelvic efferents at the caudal level were not recruited below 1000 µA.

with pudendal afferents is likely to improve any evoked voiding reflexes, as the bladder fullness signal contributes to activation in the reflex circuit [16]. Pelvic afferents are unlikely to have a detrimental effect on continence reflexes evoked by pudendal afferents [16], making concurrent pelvic and pudendal afferent activity such as that seen in the caudal location in our model a clinically useful outcome. However, efferent recruitment could interfere with reflex-mediated bladder functions. For example, if SCS intended to recruit continence reflexes simultaneously recruited the pelvic efferents that contract the bladder, bladder capacity would be reduced. Our model allows us to predict the amplitude range dominated by afferent-only recruitment, and suggests that initial nerve recruitment has a negligible efferent component. Importantly, separating afferent and efferent recruitment thresholds through SCS is experimentally difficult, illustrating one important insight gained from this model.

V. LIMITATIONS

Although the results of the computational model presented here are qualitatively and quantitatively similar to our experimental findings, the model does not contain the *dura mater*, which may affect recruitment amplitudes. Also, the computational model represents small sensory axons using an adapted MRG model rather than a true model of A-delta neurons such as that demonstrated by Graham et al [17]. In future work, we will incorporate both of these elements for a more physiologically accurate reproduction of spinal cord dynamics.

VI. CONCLUSION

We produced a functionalized model of the lumbosacral spinal cord to examine neural recruitment by SCS. This work demonstrates that it is possible to evoke substantial pudendal afferent recruitment, which is necessary for afferent-mediated bladder reflexes, without simultaneously recruiting efferents. Furthermore, models capable of exploring differences in

physiologically-relevant neural recruitment based on electrode lead placement and stimulation parameters are critical for future clinical implants. Our model simulations expose differences in the types of nerves recruited and the dynamic range between afferent and efferent recruitment at two different spinal locations.

REFERENCES

[1] M. K. Jantz *et al.*, "High-density spinal cord stimulation selectively activates lower urinary tract afferents," *Biorxiv*, p. 2021.04.30.442206, 2021, doi: 10.1101/2021.04.30.442206.
[2] C. J. Fowler, D. Griffiths, and W. C. de Groat, "The neural control of micturition.," *Nature reviews. Neuroscience*, vol. 9, no. 6, pp. 453–66, 2008, doi: 10.1038/nrn2401.
[3] J. W. Boggs, B. J. Wenzel, K. J. Gustafson, and W. M. Grill, "Frequency-dependent selection of reflexes by pudendal afferents in the cat," *J Physiol*, vol. 577, no. 1, pp. 115–126, 2006, doi: 10.1113/jphysiol.2006.111815.
[4] C. Tai, J. Wang, X. Wang, W. C. de Groat, and J. R. Roppolo, "Bladder inhibition or voiding induced by pudendal nerve stimulation in chronic spinal cord injured cats," *Neurourol Urodynam*, vol. 26, no. 4, pp. 570–577, 2007, doi: 10.1002/nau.20374.
[5] F. M. J. Martens, J. P. F. A. Heesakkers, and N. J. M. Rijkhoff, "Surgical Access for Electrical Stimulation of the Pudendal and Dorsal Genital Nerves in the Overactive Bladder: A Review," *J Urology*, vol. 186, no. 3, pp. 798–804, 2011, doi: 10.1016/j.juro.2011.02.2696.
[6] M. Capogrosso *et al.*, "A Computational Model for Epidural Electrical Stimulation of Spinal Sensorimotor Circuits," *J Neurosci*, vol. 33, no. 49, pp. 19326–19340, 2013, doi: 10.1523/JNEUROSCI.1688-13.2013.
[7] M. Kawatani, J. Nagel, and W. C. D. Groat, "Identification of neuropeptides in pelvic and pudendal nerve afferent pathways to the sacral spinal cord of the cat," *J Comp Neurol*, vol. 249, no. 1, pp. 117–132, 1986, doi: 10.1002/cne.902490109.
[8] I. Nadelhaft, W. C. de Groat, and C. Morgan, "The distribution and morphology of parasympathetic preganglionic neurons in the cat sacral spinal cord as revealed by horseradish peroxidase applied to the sacral ventral roots," *J Comp Neurol*, vol. 249, no. 1, pp. 48–56, 1986, doi: 10.1002/cne.902490105.
[9] K. Chung and R. E. Coggeshall, "The ratio of dorsal root ganglion cells to dorsal root axons in sacral segments of the cat," *J Comp Neurol*, vol. 225, no. 1, pp. 24–30, 1984, doi: 10.1002/cne.902250104.
[10] R. E. Coggeshall, J. D. Coulter, and W. D. Willis, "Unmyelinated axons in the ventral roots of the cat lumbosacral enlargement," *J Comp Neurol*, vol. 153, no. 1, pp. 39–58, 1974, doi: 10.1002/cne.901530105.
[11] C. E. Hulsebosch and R. E. Coggeshall, "An analysis of the axon populations in the nerves to the pelvic viscera in the rat," *J Comp Neurol*, vol. 211, no. 1, pp. 1–10, 1982, doi: 10.1002/cne.902110102.
[12] C. C. McIntyre, A. G. Richardson, and W. M. Grill, "Modeling the Excitability of Mammalian Nerve Fibers: Influence of Afterpotentials on the Recovery Cycle," *J Neurophysiol*, vol. 87, no. 2, pp. 995–1006, 2002, doi: 10.1152/jn.00353.2001.
[13] S. Miocinovic *et al.*, "Computational Analysis of Subthalamic Nucleus and Lenticular Fasciculus Activation During Therapeutic Deep Brain Stimulation," *J Neurophysiol*, vol. 96, no. 3, pp. 1569–1580, 2006, doi: 10.1152/jn.00305.2006.
[14] D. Sundt, N. Gamper, and D. B. Jaffe, "Spike propagation through the dorsal root ganglia in an unmyelinated sensory neuron: a modeling study," *J Neurophysiol*, vol. 114, no. 6, pp. 3140–3153, 2015, doi: 10.1152/jn.00226.2015.
[15] M. J. McGee and W. M. Grill, "Modeling the spinal pudendo-vesical reflex for bladder control by pudendal afferent stimulation," *J Comput Neurosci*, vol. 40, no. 3, pp. 283–296, 2016, doi: 10.1007/s10827-016-0597-5.
[16] J. P. Woock, P. B. Yoo, and W. M. Grill, "Mechanisms of reflex bladder activation by pudendal afferents," *Am J Physiol Regul Integ Comp Physiol*, vol. 300, no. 2, pp. R398–R407, 2011, doi: 10.1152/ajpregu.00154.2010.
[17] R. D. Graham, T. M. Bruns, B. Duan, and S. F. Lempka, "The Effect of Clinically Controllable Factors on Neural Activation During Dorsal Root Ganglion Stimulation," *Neuromodulation Technology Neural Interface*, 2020, doi: 10.1111/ner.13211.